Multimedia Tools and Applications (2019) 78:33223–33246
https://doi.org/10.1007/s11042-019-7159-6

RGB-D point cloud registration via infrared and color camera

Teng Wan[1,2] · Shaoyi Du[1,2] · Yiting Xu[1] · Guanglin Xu[1] · Zuoyong Li[2] · Badong Chen[1] · Yue Gao[3]

Received: 28 August 2018 / Revised: 3 December 2018 / Accepted: 3 January 2019 /
Published online: 13 March 2019

Abstract
The iterative closest point (ICP) algorithm is widely used for rigid registration for its simplicity and speed, but the registration is easy to fail when point sets lack of obvious structure variety, such as smooth surface and hemisphere. RGB-D information obtained from infrared camera and color camera could use color information to compensate the shapes, so we propose a precise new algorithm for RGB-D point cloud registration, which is an extension of ICP algorithm. First of all, we introduce the color information as a constraint condition to establish correct correspondences between point clouds. Secondly, to reduce the impact of noises and outliers, we use maximum correntropy criterion (MCC) to increase the robustness and accuracy. Thirdly, we add both color information and correntropy into our objective function model and solve it with ICP algorithm. Finally, the compared experiments on simulation and real datasets prove that our algorithm can align two smooth surfaces more accurate and robust than other point set registration algorithms.

Keywords Infrared and color camera · Iterative closest point · RGB-D · Maximum correntropy criterion

1 Introduction

With the development of imaging technology, multi-source sensor fusion is important in computer vision and image processing. For example, RGB-D point cloud obtained by the infrared and color

✉ Shaoyi Du
dushaoyi@gmail.com

[1] Institute of Artificial Intelligence and Robotics, School of Electronic and Information Engineering, Xi'an Jiaotong University, Xi'an, Shaanxi Province 710049, People's Republic of China

[2] Fujian Provincial Key Laboratory of Information Processing and Intelligent Control, Minjiang University, Fuzhou 350121, People's Republic of China

[3] School of Software, Tsinghua University, Beijing 100084, People's Republic of China

camera could be applied to biomedical image registration [32], simultaneous localization and mapping (SLAM) [8], 3D reconstruction [18] and vision-based autonomous driving [29] etc. Point cloud registration aims to merge point sets from different times with different views by using the information of points and restore the shape and spatial position of the objects.

In the past decades, as the collection of point sets becomes convenient, more studies focused on shape registration. Besl et al. proposed the ICP algorithm [4], which provides a reliable tool for point set registration, so a lot of researches are based on this algorithm. The ICP algorithm can get much fast speed for point set registration, and does not need to extract the features of the point sets or preprocess the data point set. In recent years, research on ICP algorithm has focused on speed and robustness and many variant algorithms are proposed.

To improve registration speed of the ICP algorithm, there are three aspects (select, match, minimize) can be optimized. Firstly, to accelerate the points selecting speed, Kim et al. [20] used a coarse-to-fine method to accelerate registration process, which combined hierarchical model point selection (HMPS) method with logarithmic data point search (LDPS) method. Greenspan et al. [15] presented an innovative ICP algorithm based on approximate k-d tree, which may have a better convergence when the moderately large point sets have outliers. Yan et al. [35] proposed a new method called pre-computed voxel closest neighbors to accelerate the registration, which computing the data structure before matching. Nchter et al. [26] proposed an improved search method called cached *k*-d trees to accelerate registration, which is 50% faster than traditional *k*-d tree based ICP algorithm. Secondly, to reduce the matching time, Benjemaa et al. [3] used a multi-z-buffer technique to accelerate the establish process of correspondence between overlapping surfaces. Rusinkiewicz et al. [28] proposed a projection-based ICP algorithm with uniform sampling of normal space which can align two range images in tens of milliseconds. Censi [5] proposed the point-to-line ICP (PLICP) algorithm, which use the minimum distance between the current point and the nearest two points when finding the correspondence. However, PLICP algorithm is not robust with large initial displacement errors. Thirdly, to increase convergence speed, Granger et al. [14] regarded the rigid transformation as Maximum-Likelihood (ML) estimation and used Expectation Maximization (EM) principles to solve this estimation. Belshaw et al. [2] proposed a variant ICP algorithm with hardware acceleration called field programmable gate array (FPGA), which can increase the registration speed by 5 times than K-D tree method.

To enhance the accuracy and robustness of the ICP algorithm, there are several works focus on initial value, noises and outliers, error metric. Firstly, in order to solve the initial value problem, He et al. [16] proposed a variant ICP algorithm based on geometric features, which can converge without a good initial value. Du et al. [9] presented a robust registration algorithm which use the characteristics of the corners in the image to get robust results. Secondly, to solve the noises and outliers problem, Masuda et al. [23] presented a robust ICP algorithm with random sampling and least median of squares (LMS) estimator via classifing the point sets into four categories and LMS has good exclusion characteristics for outliers. Kaneko et al. [19] used a modified M-estimation iteration to establish correspondences with bi-weighting coefficients, but the point sets need good initial position. Silva et al. [30] used hybrid genetic algorithm to combine with evaluation metric based on surface interpenetration and robust to significant noise in point sets. Ridene et al. [27] proposed a robust ICP algorithm with RANSAC method and adaptive dynamic threshold to reduce the outliers, which is based on the fusion of heterogeneous. Xu et al. [34] proposed an MCC (maximum correntropy criterion) based robust registration algorithm, which can effectively reduce the impact of noises and outliers on registration accuracy. Thirdly, to solve the error metric problem, Fitzgibbon [13] proposed a new registration method with the Levenberg-

Marquardt algorithm to minimizing the registration error, and get both faster and more robust than standard ICP algorithm. Chetverikov et al. [6] proposed the trimmed ICP based algorithm with the Least Trimmed Squares approach and the algorithm have good robustness for erroneous and incomplete point set. Myronenko et al. [25] presented a probabilistic method with Gaussian mixture model (GMM) centroids registration, called the Coherent Point Drift (CPD) algorithm and used maximum likelihood estimation to solve the probability density estimation problem. Du et al. [10, 11] used Gaussian model and expectation maximization (EM) to obtain more robust registration results with a probability ICP framework.

The above algorithms focus on the structural information but ignore other information of point sets, like color, texture and so on. Fortunately, with the development of camera, we can get the color and depth information simultaneously. This technological innovation of RGB-D camera motivates more and more researches on RGB-D point cloud registration. Hao et al. [24] presented the 4D ICP algorithm, which contains the coordinate and hue information, to get correct correspondences between point sets. However, the algorithm is not robust enough to noises and outliers because all points participate in the registration process. Korn et al. [21] proposed a plane to plane ICP variant with Lab color space and use *k*-d tree search algorithm to match corresponding points, but this algorithm is susceptible to light. Danelljan et al. [7] proposed a probabilistic registration framework based on the joint distribution and color information. However, the above two algorithms do not research the registration to weak structure point sets, like smooth surface or hemisphere. To solve this problem, we present a precise registration algorithm for weak structure point sets. By introducing color information and correntropy, a constrained objective function is established. Then we propose an improved ICP algorithm to solve this optimization issue. The experimental results demonstrate that our algorithm can register two smooth surface with good precision and robustness.

The rest of this paper is structured as follows. In section 2, we introduce the ICP algorithm briefly and propose its defects in registration of smooth surface. In section 3, we present our algorithm and analyze the rationality and feasibility of the algorithm with mathematical expression. In section 4, we test our algorithm in both simulation and real data experiments and analyze the experimental results. In section 5, we give the conclusion.

2 Problem statement

The traditional ICP algorithm registers two point sets precisely via several iterations when the point sets have good initial value. Here, we introduce the algorithm briefly [4]. Given two *m*-dimension point sets in $\mathbb{R}^m$, the data point set $X \triangleq \left\{\overrightarrow{x}_i\right\}_{i=1}^{N_x} (N_x \in \mathbb{N})$ and the target point set $Y \triangleq \left\{\overrightarrow{y}_j\right\}_{j=1}^{N_y} \left(N_y \in \mathbb{N}\right)$. Then, the ICP algorithm calculates the rigid transformation between the pairs of point set iteratively. Here, a least squares (LS) criterion optimization method is applied and the objective function is:

$$\min_{R,\ \overrightarrow{t},c(i)\in\left\{1,2,\cdots,N_y\right\}} \sum_{i=1}^{N_x} \left\| \left(R\overrightarrow{x}_i + \overrightarrow{t}\right) - \overrightarrow{y}_{c(i)} \right\|_2^2 \qquad s.t. \qquad \mathrm{R}^{\mathrm{T}}\mathrm{R} = \mathrm{I}_m, \det(\mathrm{R}) = 1 \tag{1}$$

where $R \in \mathbb{R}^{m \times m}$ is a rotation matrix, and $\overrightarrow{t} \in \mathbb{R}^m$ is a translation vector.

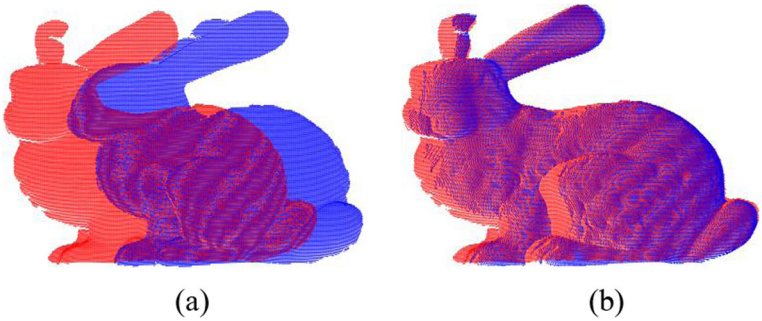

Fig. 1 The registration of ICP. (a) The initial position of two point sets. (b) The registration results of ICP

Because the point sets $\vec{x}_i$ and $\vec{y}_i$ are known, the ICP algorithm computes the rotation matrix R and translation vector $\vec{t}$ iteratively. At the k^{th} iteration, it contains two basic steps:

First, establishing the correspondence between two point sets:

$$c_k(i) = \underset{c(i)\in\{1,2,\cdots,N_y\}}{\operatorname{argmin}} \left\| \left(R_{k-1}\vec{x}_i + \vec{t}_{k-1}\right) - \vec{y}_{c(i)} \right\|_2^2, i = 1,2,\cdots,N_x \tag{2}$$

Second, computing the rotation matrix R and translation vector $\vec{t}$:

$$\left(R_k, \vec{t}_k\right) = \underset{R^TR=I_m,\det(R)=1,\ \vec{t}}{\operatorname{argmin}} \sum_{i=1}^{N_x} \left\| R\vec{x}_i + \vec{t} - \vec{y}_{c_k(i)} \right\|_2^2 \tag{3}$$

We repeat the above two steps until the algorithm reaches some certain qualifications such as maximum iteration number or minimum error value. After that, the point sets in different spatial positions will be unified into the same coordinate system and one registration result is shown as Fig. 1. We can find that the blue rabbit aligns to the red rabbit via a rigid transformation in good accuracy and robustness.

3 RGB-D point cloud registration based on correntropy

However, ICP algorithm is easily failed when the point sets are lack of obvious structural features, like smooth surface and hemisphere. In this case, the correct correspondences based on the mean square error (MSE) between point clouds are difficult to establish, which are shown in Fig. 2.

3.1 RGB-D registration problem

Obviously, for smooth surface point sets, it is not enough to use the Euclidean distance measurement alone to get the correct registration result. Fortunately, the RGB-D camera provides the color and structure information of the object simultaneously. Therefore, we employ color information to improve the registration accuracy.

Firstly, we use color information of each point to get correct correspondences between point clouds. Secondly, the color information is translated from red, green, blue (RGB) color space to hue, saturation, value (HSV) color space to reduce the effects of lighting. Thirdly, we

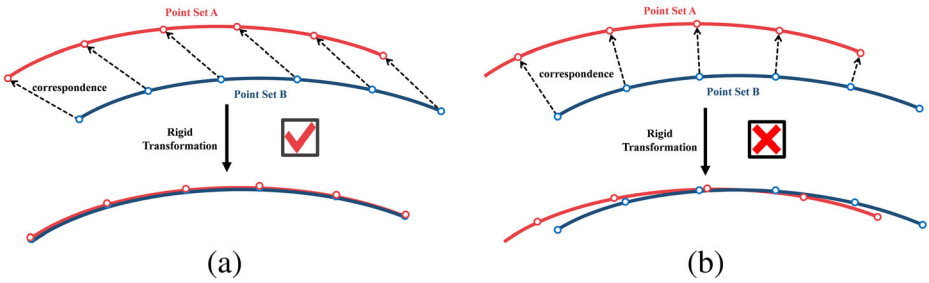

Fig. 2 Smooth surface point sets registration. **a** The expected registration results. **b** The registration result of ICP algorithm

remove points that may affect registration accuracy based on the amount of points in each color.

3.1.1 Establish the correspondences with color-assisted

To smooth surface point sets, the color information offers a new evaluation criterion of "closest points" in both Euclidean space and color space. In Fig. 3, with color guided, we have more accuracy registration results with a reasonable correspondence in each iteration. This way of searching correspondences is more like human behavior; it means that when we register two parts of one object, we align them based on shape and color simultaneously.

3.1.2 Reduce the effects of lighting

To reduce the effects of lighting, we transform color point sets from red-green-blue, (RGB) color space to hue-saturation-value (HSV) color space. Then, we remove the saturation and value to wipe off the effect of lighting, and only use the hue value to find the correspondences and calculate the rigid transformation. As we known, the hue value can better reflect the essence of color and is not sensitive to changes of illumination. To prove the hue can reduce the impact of light, we test the change of RGB value and hue value in different lighting conditions as shown in Fig. 4.

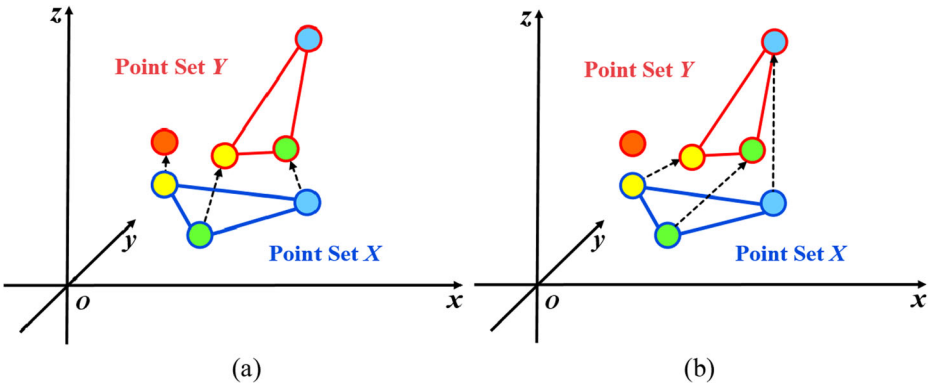

Fig. 3 Establish correspondence between two point sets with color-assisted. **a** Without color-assisted. **b** With color-assisted

Fig. 4 The change rate of RGB value and hue in different lighting conditions. **a** A cup in different light conditions. **b** The change rate of red, green, blue and hue values

Considering the magnitude of RGB value and hue value in different levels, we normalize them with the formula $z = (x - y)/(x + y)$, where z is the change rate of one value and x and y is the color value of the same pixels points in different lighting conditions.

From Fig. 4b, we choose five pixels of cup image randomly in light and dark Illuminance. In each pixel, we can find that the hue value gets the smaller change rate than RGB in different lighting conditions. Here, a more reliable and common element is generated to improve the registration accuracy for weak structure point sets. Compared with RGB value, the application of hue also decreases the computational complexity because the hue reduces the calculation of three values to one.

3.1.3 Point selection via rejecting the noise and background points

We have the hue value of each point, but we still cannot directly use them. After lots of experiments, we find that the color-assisted registration will fail easily if the number of one kind of color point is too big or too small. When the number of one color point is smaller than a threshold a, we regard them as noise and if the number exceeds a threshold b, we consider them as background. The noise and background points should delete before registration and one filtered result is shown in Fig. 5. In this experiment, the points are divided into eight color categories as red, orange, yellow, green, cyan, blue, purple, magenta, and the percentages of points in different color are 0.61, 2.34, 2.59, 17.74, 2.19, 68.33, 2.79, 2.24. Therefore, according to the point choice criterion, only the green points are retained, and the results are shown in Fig. 5c. In addition, we give much more examples in Fig. 6.

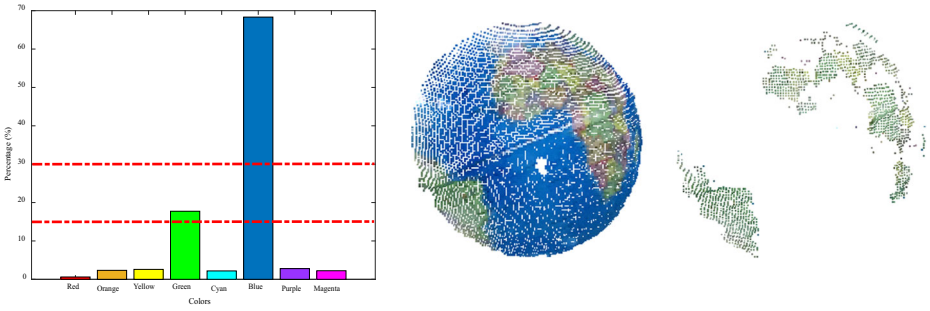

Fig. 5 Delete the noise and background points based on the color distribution. **a** The color distribution. **b** The original point sets. **c** The filtered point sets

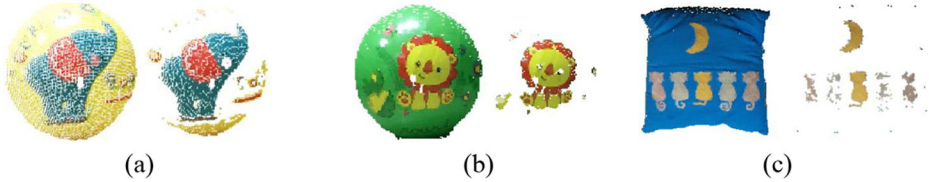

Fig. 6 The filtered point sets. **a** Ball1. **b** Ball2. **c** Pillow

We can find that while obtaining stable color elements, we get more structural information simultaneously. Due to the color filter, many structurally smooth objects are forced to separate themselves and more independent sub-point-set offer more edge and structured information. Moreover, the object function of RGB-D registration model can be expressed as follow:

$$\min_{R,\vec{t},c(i)\in\{1,2,\cdots,N_y\}} \sum_{i=1}^{N_x}\left(\left\|\left(R\vec{x}_i+\vec{t}\right)-\vec{y}_{c(i)}\right\|_2^2+w\left(h_i^x-h_{c(i)}^y\right)^2\right) \quad s.t. \quad \mathrm{R}^{\mathrm{T}}\mathrm{R}=\mathrm{I}_m, \det(\mathrm{R})=1 \tag{4}$$

the hue values of the data point sets $X\triangleq\left\{\vec{x}_i\right\}_{i=1}^{N_x}\left(N_x\in\mathbb{N}\right)$ and the target point set $Y\triangleq\left\{\vec{y}_j\right\}_{j=1}^{N_y}$ $\left(N_y\in\mathbb{N}\right)$ are denoted as h_i^x and h_j^y respectively.

3.2 RGB-D registration based on maximum correntropy criterion

After point selection, the weak structure point set is turned into a strong structure point set, but more noises and outliers appeared and those points influence the accuracy of registration directly. To overcome this problem, we introduce the maximum correntropy criterion (MCC).

3.2.1 The correntropy

A brief introduction of correntropy is given, between the data point sets $X\triangleq\left\{\vec{x}_i\right\}_{i=1}^{N_x}\left(N_x\in\mathbb{N}\right)$ and the target point sets $Y\triangleq\left\{\vec{y}_j\right\}_{j=1}^{N_y}\left(N_y\in\mathbb{N}\right)$, the correntropy is denoted as:

$$g\left(\vec{x},\vec{y}\right)=\sum_{i=1}^{N_x}\exp\left(-\left\|\vec{x}_i-\vec{y}_{c(i)}\right\|_2^2/\left(2\sigma^2\right)\right) \tag{5}$$

where $c(\cdot)$ is the correspondence index of the target point and σ is the variance. The distribution of correntropy function and MSE function are shown in Fig. 7a and b respectively.

In Fig. 7b, MSE increases in square with respect to the distance between x and y, which means that even the distance is large, they still affect the total error. On the contrary, MCC magnifies the change of distance between two point sets exponentially as shown in Fig. 7a, which means smaller the difference of two points is, larger the value of the correntropy is. Conversely, if one corresponding point set is outlier, the correntropy of them will be close to 0, and if it is shape noises, it will get much smaller error than the normal point sets. Therefore, the correntropy is resistance to the shape noises and outliers effectively.

As show in (5), if the point sets X and Y have the smallest distance, we need to maximize the value of $g\left(\vec{x},\vec{y}\right)$. Hence, according to the ICP registration framework based on maximum correntropy criterion [34], the objective function can be expressed as:

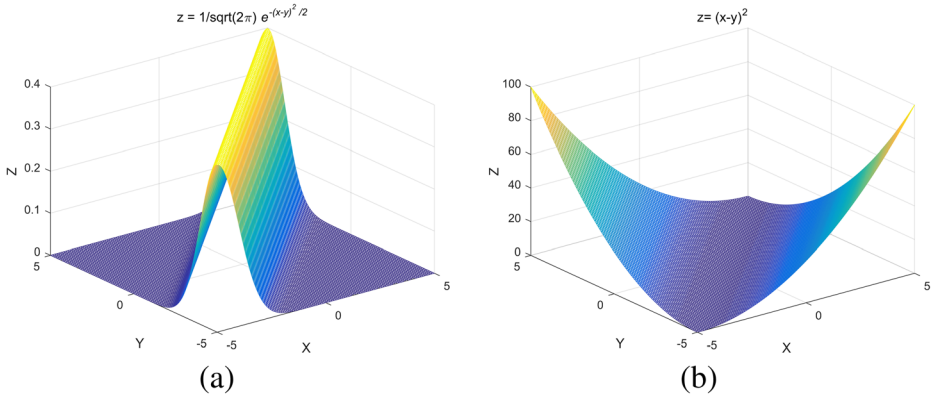

Fig. 7 The distribution of correntropy function and MSE function. **a** The distribution of correntropy function. **b** The distribution of MSE function

$$\max_{\substack{R,\vec{t}\\ c(i)\in\{1,2,\cdots,N_y\}}} \sum_{i=1}^{N_x}\exp\left(-\frac{\left\|\left(R\vec{x}_i+\vec{t}\right)-\vec{y}_{c(i)}\right\|_2^2}{2\sigma^2}\right) \quad s.t. \quad \mathrm{R}^T\mathrm{R}=\mathrm{I}_m, \det(R)=1 \tag{6}$$

MCC-based algorithm fully considers the characteristics of point sets and eliminates outliers while reducing the impact of shape noises. Even though we have strengthened the structure characteristic of point sets, we still neglect the feature of color space. The registration is easy to fail when the shape of point sets is lack of obvious change. Therefore, we introduce the color information to find the correct correspondence and shortest distance in both Euclidean space and color space. Similarly, in MCC framework, we also need color information to improve the accuracy of registration and the objective function is denoted as follow:

$$\max_{\substack{R,\vec{t}\\ c(i)\in\{1,2,\cdots,N_y\}}} \sum_{i=1}^{N_x}\exp\left(-\frac{\left\|\left(R\vec{x}_i+\vec{t}\right)-\vec{y}_{c(i)}\right\|_2^2+w\left(h_i^x-h_{c(i)}^y\right)^2}{2\sigma^2}\right) \quad s.t. \quad \mathrm{R}^T\mathrm{R}=\mathrm{I}_m, \det(R)=1 \tag{7}$$

where ω is a weight of hue value.

4 The proposed algorithm

In this section, our new ICP algorithm is introduced and its derivation and theoretical analysis are carried out in detail.

4.1 A new ICP algorithm

With color-assisted, we transform the traditional 3D point cloud registration problem to 4D registration problem. For example, one point $\vec{v}_i=\{x_i,y_i,z_i\}$ in a point set $V\triangleq\left\{\vec{v}_i\right\}_{i=1}^{N_v}$ $(N_v\in\mathbb{N})$ can be rewritten as $\vec{v}_i=\{x_i,y_i,z_i,wh_i\}$. The $\{x_i,y_i,z_i\}$ is the spatial coordinates of point $\vec{v}_i.w$ is the weight of the hue value h_i.

Similar to the traditional ICP algorithm, we need two steps to calculating the rigid transformation between the data point sets $X \triangleq \left\{ \overrightarrow{x}_i \right\}_{i=1}^{N_x} (N_x \in \mathbb{N})$ and the target point sets $Y \triangleq \left\{ \overrightarrow{y}_j \right\}_{j=1}^{N_y} (N_y \in \mathbb{N})$.

Step 1: we establish the correspondence in $(k-1)^{th}$ iteration:

$$c_k(i) = \underset{c(i) \in \left\{1,2,\cdots N_y\right\}}{\operatorname{argmin}} \left(\left\| \left(R_{k-1} \overrightarrow{x}_i + \overrightarrow{t}_{k-1} \right) - \overrightarrow{y}_{c(i)} \right\|_2^2 \right) \tag{8}$$

this step can divide into three parts:

(1) We compute the distance d_{ij} between two points $\overrightarrow{x}_i = \{x_i, y_i, z_i, wh_i\}$ and $\overrightarrow{y}_j = \left\{x_j, y_j, z_j, wh_j\right\}$, which is defined as follows.

$$d_{ij} = \sqrt{\left(x_i - x_j\right)^2 + \left(y_i - y_j\right)^2 + \left(z_i - z_j\right)^2 + w\left(h_i - h_j\right)^2} \tag{9}$$

(2) According to the closest point that point set $X \triangleq \left\{ \overrightarrow{x}_i \right\}_{i=1}^{N_x} (N_x \in \mathbb{N})$ finds in point set $Y \triangleq \left\{ \overrightarrow{y}_j \right\}_{j=1}^{N_y} (N_y \in \mathbb{N})$, we can establish the correspondences $\{(i, c_k(i)) | i=\}$.

Step 2: the rigid transformation is decomposed into the rotation matrix R and translation vector $\overrightarrow{t}$ and the formula is expressed as follow:

$$\left(\mathrm{R}_k, \overrightarrow{t}_k \right) = \underset{R^T R = \mathrm{I}_m, \det(R)=1, \overrightarrow{t}}{\operatorname{argmax}} \sum_{i=1}^{N_x} \exp\left(- \frac{\left\| \left(R \overrightarrow{x}_i + \overrightarrow{t} \right) - \overrightarrow{y}_{c(i)} \right\|_2^2 + w\left(h_i^x - h_{c(i)}^y \right)^2}{2\sigma^2} \right) \tag{10}$$

Our algorithm repeats the above two steps until it converges to a local maximum or reaches the maximum number of iterations.

4.2 Rigid transformation computation

4.2.1 Translation computation

Similar to the traditional ICP algorithm, we need to compute the rotation matrix R and translation vector $\overrightarrow{t}$ respectively. Considering the independence of these two quantities, we can simplify these formulas firstly. Therefore, to any two point sets $\left\{ \overrightarrow{x}_i \right\}_{i=1}^{N}$ and $\left\{ \overrightarrow{y}_i \right\}_{i=1}^{N}$, the objective function is

$$F\left(\overrightarrow{t}\right)=\sum_{i=1}^{N}\exp\left(-\frac{\left\|\left(R\overrightarrow{x}_i+\overrightarrow{t}\right)-\overrightarrow{y}_i\right\|_2^2+w\left(h_i^x-h_i^y\right)^2}{2\sigma^2}\right) \tag{11}$$

If $F\left(\overrightarrow{t}\right)$ gets the minimum value, it must meet the following condition$dF\left(\overrightarrow{t}\right)/d\overrightarrow{t}=0$. Next, the formula can be obtained by deriving $F\left(\overrightarrow{t}\right)$:

$$\frac{dF\left(\overrightarrow{t}\right)}{d\overrightarrow{t}}=\sum_{i=1}^{N}\left(-\frac{\mathrm{R}\overrightarrow{x}_i+\overrightarrow{t}-\overrightarrow{y}_i}{\sigma^2}e^{-\frac{\left\|\mathrm{R}\overrightarrow{x}_i+\overrightarrow{t}-\overrightarrow{y}_i\right\|_2^2+w\left(h_i^x-h_i^y\right)^2}{2\sigma^2}}\right) \tag{12}$$

Here, we set $s(i)=e^{-\frac{\left\|\mathrm{R}\overrightarrow{x}_i+\overrightarrow{t}-\overrightarrow{y}_i\right\|_2^2+w\left(h_i^x-h_i^y\right)^2}{2\sigma^2}}$ and let $dF\left(\overrightarrow{t}\right)/d\overrightarrow{t}=0$,so we can get:

$$\overrightarrow{t}=\left(\sum_{i=1}^{N}\left(\overrightarrow{y}_i-\mathrm{R}\overrightarrow{x}_i\right)s(i)\right)/\sum_{i=1}^{N}s(i) \tag{13}$$

4.2.2 Rotation transformation computation

Substitute $\overrightarrow{t}_k$ into formula (10), we can get:

$$\mathrm{R}_k=\underset{R^TR=\mathrm{I}_m,\det(R)=1}{\operatorname{argmax}}\sum_{i=1}^{N_x}\exp\left(-\frac{\left\|R\overrightarrow{m}_i-\overrightarrow{n}_i\right\|_2^2}{2\sigma^2}\right) \tag{14}$$

where $\overrightarrow{m}_i=\overrightarrow{x}_i-\left(\sum_{i=1}^{N}s_k(i)\overrightarrow{x}_i\right)/\sum_{i=1}^{N}s_k(i)$ and $\overrightarrow{n}_i=\overrightarrow{y}_{c_k(i)}-\left(\sum_{i=1}^{N}s_k(i)\overrightarrow{y}_{c_k(i)}\right)/\sum_{i=1}^{N}s_k(i)$.

After the simplified formula is given, we can calculate the rotation matrix in many ways, such as (Singular Value Decomposition) SVD method [1], quaternion method [12], orthogonal matrix method [17], double quaternion method [33] and so on. In this paper, we choose SVD to derive the rotation matrix as its simplicity.

To facilitate calculating rotation matrix with SVD method, we set M and N as $N_x\times n$ matrices where each row contains $\overrightarrow{m}_i$ and $\overrightarrow{n}_i$ respectively. Therefore, the formula (15) can be expressed as:

$$\mathrm{R}_k=\underset{R^TR=\mathrm{I}_m,\det(R)=1}{\operatorname{argmax}}1_{N_x}^TG\left(\mathrm{N}-\mathrm{M}R^T\right) \tag{15}$$

where $1_{N_x}^T$ is a row vector where every element is 1 and $G\left(\mathrm{N}-\mathrm{M}R^T\right)=\overrightarrow{g}$ is a column vector with $G_i=\exp\left(-\frac{\left\|R\overrightarrow{m}_i-\overrightarrow{n}_i\right\|_2^2}{2\sigma^2}\right)$ in each row. To solve the optimization problems with constraints, we choose Lagrangian multiplier method. Therefore, we defined the objective function as:

$$L(\mathrm{R},K,\eta)=1_{N_x}^TG(\mathrm{R})+tr\left(K\left(\mathrm{R}^T\mathrm{R}-\mathrm{I}_n\right)\right)+\eta(\det(\mathrm{R})-1) \tag{16}$$

Here, K and η are Lagrange multiplier, K is a $n \times n$ symmetric matrix and η is a number. *tr* is the trace of the matrix. To maximize the objective function, we need to solve the partial derivative of R, K and η, and set the derivative as 0. Therefore, we can get the following equation set:

$$\frac{\partial L}{\partial \mathrm{R}} = -\frac{1}{\sigma^2}\left(\mathrm{M}^T D\left(\overrightarrow{g}\right)\mathrm{MR} - \mathrm{M}^T D\left(\overrightarrow{g}\right)\mathrm{N}\right) + 2\mathrm{KR} + \eta\mathrm{R} = 0 \tag{17}$$

$$\frac{\partial L}{\partial \mathrm{K}} = \mathrm{R}^T\mathrm{R} - \mathrm{I}_m = 0 \tag{18}$$

$$\frac{\partial L}{\partial \eta} = \det(\mathrm{R}) - 1 = 0 \tag{19}$$

where $D\left(\overrightarrow{g}\right) = diag\left(\overrightarrow{g}\right)$ is a diagonal matrix.

Then, let $\mathrm{L}' = -\frac{1}{\sigma^2}\mathrm{M}^T D\left(\overrightarrow{g}\right)\mathrm{M} + 2\mathrm{K} + \eta$. According to the Eq. (17), we can get:

$$\mathrm{L}'\mathrm{R} = -\frac{1}{\sigma^2}\mathrm{M}^T D\left(\overrightarrow{g}\right)\mathrm{N} \tag{20}$$

Now we can use SVD to solve L'R, and then we can get:

$$\mathrm{L}'\mathrm{R} = \mathrm{U}\Lambda\mathrm{V}^T \tag{21}$$

Here, U and V are unitary matrix. Λ is a $n \times n$ diagonal matrix, where every element is non-negative and the diagonal elements in the matrix are arranged in descending order that is $\lambda_1 \geq \lambda_2 \geq \ldots \geq \lambda_{n-1} \geq \lambda_n \geq 0$. Then, we transpose the formula (20) on both two sides and get:

$$\mathrm{R}^T\mathrm{L}'^T = -\frac{1}{\sigma^2}\left(\mathrm{M}^T D\left(\overrightarrow{g}\right)\mathrm{N}\right)^T = \mathrm{V}\Lambda\mathrm{U}^T \tag{22}$$

Next, left multiply both sides of formula (22) by formula (21). According to $\mathrm{R}^T\mathrm{R} = \mathrm{I}_m$, we can get:

$$\mathrm{L}'^2 = \mathrm{U}\Lambda\mathrm{V}^T\mathrm{V}\Lambda\mathrm{U}^T \tag{23}$$

Obviously, $\mathrm{L}'^2\mathrm{L}' = \mathrm{L}'\mathrm{L}'^2$, the same orthogonal matrix can be simplified as a diagonal matrix form, and we can get:

$$\mathrm{L}' = \mathrm{U}\Lambda D\left(\overrightarrow{d}\right)\mathrm{U}^T \tag{24}$$

Here, $D\left(\overrightarrow{d}\right) = diag\left(\overrightarrow{d}\right)$ is a diagonal matrix and d_i equals to 1 or − 1. As shown in formula (24) we can get this:

$$\det\left(\mathrm{L}'\right) = \det\left(\mathrm{U}\Lambda\mathrm{D}\left(\overrightarrow{d}\right)\mathrm{U}^T\right) = \det(\Lambda)\det\left(D\left(\overrightarrow{d}\right)\right) \tag{25}$$

In the other hand, according to formula (20), we can get:

$$\det\left(\mathrm{L}^{'}\right) = \det\left(\mathrm{L}^{'}\right)\det(\mathrm{R}) = \det\left(\mathrm{L}^{'}\mathrm{R}\right) \tag{26}$$

Combine the above two formulas and we can get:

$$\det(\Lambda)\det\left(D\left(\overrightarrow{d}\right)\right) = \det\left(L^{'}\mathrm{R}\right) \tag{27}$$

Because of $\det(\Lambda) = \lambda_1\lambda_2 \ldots \lambda_n \geq 0$, if $\det(L^{'}\mathrm{R}) > 0$, $\det\left(D\left(\overrightarrow{d}\right)\right) = 1$. If $\det(L^{'}\mathrm{R}) < 0$, $\det\left(D\left(\overrightarrow{d}\right)\right) = -1$. Then, left multiplying the formula (21) and we can get:

$$\mathrm{R} = \left(\mathrm{U}\Lambda D\left(\overrightarrow{d}\right)\mathrm{U}^{T}\right)^{-1}\mathrm{U}\Lambda\mathrm{V}^{T} = \mathrm{U}D\left(\overrightarrow{d}\right)^{-1}\mathrm{V}^{T} \tag{28}$$

In summary, at the k^{th} iteration, the rotation matrix R_k can be expressed as:

$$\mathrm{R}_k = \mathrm{U}D\left(\overrightarrow{d}\right)^{-1}\mathrm{V}^{T} \tag{29}$$

where $D\left(\overrightarrow{d}\right)^{-1} = \left\{ \begin{matrix} \mathrm{I}_n & \det\left(\mathrm{M}^{T}D\left(\overrightarrow{g}\right)\mathrm{N}\right) > 0 \\ diag(1,1,\ldots,-1) & \det\left(\mathrm{M}^{T}D\left(\overrightarrow{g}\right)\mathrm{N}\right) < 0 \end{matrix} \right.$. After R_k is computed, we can get $\overrightarrow{t}_k$ as follow:

$$\overrightarrow{t}_k = \frac{\sum_{i=1}^{N_x}\left(\overrightarrow{y}_{c_k(i)} - \mathrm{R}_k\overrightarrow{x}_i\right)s(i)}{\sum_{i=1}^{N_x}s(i)} \tag{30}$$

After the derivation, our algorithm is given in above section, our proposed algorithm is summarized as follows.

4.3 Theory analysis

4.3.1 Proof of convergence

Even though our algorithm cannot guarantee the final rigid transformation will be found in one-step, the process can be implemented in a stepwise approach. Moreover, because of the difference of objective function, the convergence property of our algorithm is different from ICP algorithm. Now, we proof the convergence property of our algorithm in details.

Theorem 1 Under the maximum correntropy criterion, the ICP algorithm based on the correlation entropy monotonically converges to a local maximum.

Proof Given two RGB-D point set $X \triangleq \left\{\overrightarrow{x}_i\right\}_{i=1}^{N_x}$ and $Y \triangleq \left\{\overrightarrow{y}_i\right\}_{i=1}^{N_y}$, the rotation matrix and translation vector are R_{k-1} and $\overrightarrow{t}_{k-1}$, let $\overrightarrow{v}_{i,k-1} \triangleq \mathrm{R}_{k-1}\overrightarrow{x}_i + \overrightarrow{t}_{k-1}$, so the correntropy between two point sets is denoted as:

$$\delta_k = \sum_{i=1}^{N_x} \exp\left(-\left(\left\|\overrightarrow{v}_{i,k-1} - \overrightarrow{y}_{c_k(i)}\right\|_2^2 + w\left(h_i^x - h_i^y\right)^2\right)/\left(2\sigma^2\right)\right) \tag{31}$$

To reduce the registration error, we need to increase the value of correntropy to obtain a correct rigid transformation. Therefore, we can get the correntropy:

$$\theta_k = \sum_{i=1}^{N_x} \exp\left(-\left(\left\|\mathrm{R}_k \overrightarrow{x}_i + \overrightarrow{t}_k - \overrightarrow{y}_{c_k(i)}\right\|_2^2 + w\left(h_i^x - h_i^y\right)^2\right)/\left(2\sigma^2\right)\right) \tag{32}$$

Owing to $\left(\mathrm{R}_k, \overrightarrow{t}_k\right)$ calculated by formula (10), we can get $N_x \geq \theta_k \geq \delta_k$. Then, we let $\overrightarrow{v}_{i,k} \triangleq \mathrm{R}_k \overrightarrow{x}_i + \overrightarrow{t}_k$ and the.

Correntropy is denoted as:

$$\delta_{k+1} = \sum_{i=1}^{N_x} \exp\left(-\left(\left\|\overrightarrow{v}_{i,k} - \overrightarrow{y}_{c_{k+1}(i)}\right\|_2^2 + w\left(h_i^x - h_i^y\right)^2\right)/\left(2\sigma^2\right)\right) \tag{33}$$

because of the new correspondence $c_{k+1}(i)$ is established by formula (9), $\left\|\overrightarrow{v}_{i,k} - \overrightarrow{y}_{c_{k+1}(i)}\right\|_2^2 \leq \left\|\mathrm{R}_k \overrightarrow{x}_i + \overrightarrow{t}_k - \overrightarrow{y}_{c_k(i)}\right\|_2^2$ and we can obtain $N_x \geq \delta_{k+1} \geq \theta_k$. Repeat above steps and we can get $N_x \geq \theta_{k+1} \geq \delta_{k+1} \geq \theta_k \geq \delta_k \geq \ldots \geq \theta_1 \geq \delta_1 \geq 0$. Therefore, after several iterations, our algorithm will converge to a local maximum but cannot automatically converge to global extremum because the objective function cannot find the derivative.

4.3.2 Parameter discussion

In our algorithm, three parameters directly affect the accuracy of the algorithm. Firstly, the effect of hue value is reflected in the assignment of weight w. If the weight of hue value is too large, the coordinate information of the point set will be ignored. If the weight of hue value is too small, our algorithm is equal to the ICP algorithm based on maximum correntropy criterion [34]. Therefore, a suitable weight is set to make that coordinate and hue value have the same effect on finding the nearest point. In this paper, we set the value of the weight to be 25. Secondly, the proposed algorithm will fail when the number of one kind of color point is too large or too small. Therefore, we set the minimum threshold a and maximum threshold b to limit it. In order to obtain accurate registration results, we set thresholds a and b as 5 and 30 respectively. Thirdly, the value of variable σ in the correntropy also affects the accuracy of the algorithm. When σ become bigger, the shape of regression curve will be sharper. In contrast, when σ become smaller, the shape of regression curve will be more gentle. In order to get the best outlier rejection, we set σ as 2.5 in the paper.

5 Experimental results

In this section, we test our algorithm on simulation and real dataset to verify the convergence and registration accuracy of our algorithm. The simulation datasets, RGB-D scenes dataset v2 [22] and RGB-D SLAM Dataset [31], are provided by University of Washington (UW) and

Table 1 Comparison of 3D simulation results with rotation

Datasets	Error	Algorithms			
		ICP	HaICP	MccICP	OURS
Rugby	ε_R	7.96	7.77	0.21	1.55e-30
	$\varepsilon_{\vec{t}}$	1.54	1.61	0.04	4.36e-31
Food can	ε_R	7.85	7.82	0.36	1.68e-30
	$\varepsilon_{\vec{t}}$	1.44	1.43	0.05	5.29e-31
Soda can	ε_R	7.83	7.95	0.20	7.28e-05
	$\varepsilon_{\vec{t}}$	1.60	1.65	0.03	8.10e-06
Bag	ε_R	0.50	0.52	1.27	2.13e-03
	$\varepsilon_{\vec{t}}$	0.01	0.01	0.04	5.27e-03

Technische Universität München (TUM) respectively. We use Microsoft Kinect V2 to build the real dataset. Moreover, we compare our algorithm with other three registration methods, which are ICP algorithm [4], Hue-assist ICP (HaICP) algorithm (4D ICP) [24] and maximum correntropy criterion ICP (MccICP) algorithm [34].

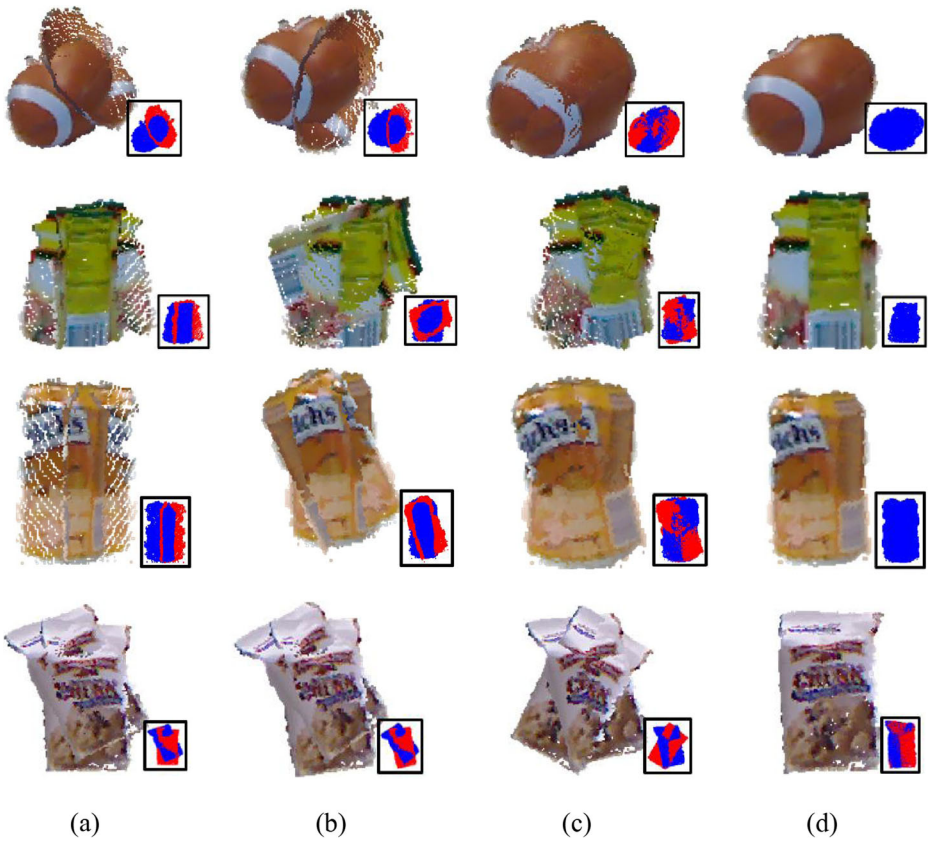

Fig. 8 The registration results. **a** ICP. **b** HaICP. **c** MccICP. **d** OURS

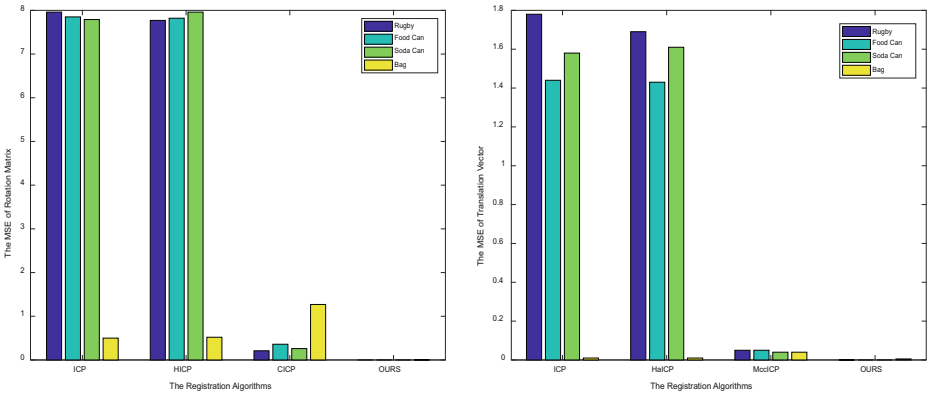

Fig. 9 The registration results. **a** The MSE of rotation matrix. **b** The MSE of translation vector

5.1 Simulation experiments

In simulation experiments, we select the point sets with weak structure feature, such as a side of food can, soda can, rugby, basketball and football. We rotate the data point set along the z axis of spatial coordinates with random degrees from 0 to 60 to obtain the target point sets and the rigid transformation R and $\overrightarrow{t}$ is known. Here, we use $\varepsilon_R = \|R_t - R\|_2$ and $\varepsilon_{\overrightarrow{t}} = \left\| \overrightarrow{t}_t - \overrightarrow{t} \right\|_2$ to determine if the registration is successful and R_t, $\overrightarrow{t}_t$ are obtained by registration algorithm. The experimental results and error comparison are shown in Table 1, Figs. 8 and 9, respectively. To distinguish whether the registration is successful, we add the registration results between data point set (blue) and target point set (red) in the bottom right corner.

In Table 1, Figs. 8 and 9, we may find that our method could get much smaller errors than the other methods, and our algorithm obtains the best registration results. Firstly, without color guided, in the ICP algorithm, the wrong correspondences between two point sets are established because the points only find the closest points in the Euclidean metric space, which may cause incorrect registration results. Secondly, with color guided, the HaICP algorithm can find the correct correspondences within two point sets, which the points can find other closest points in both Euclidean metric space and color space. However, due to the noise and background points are existed and the traditional MSE (mean-square error) metrics does not have the ability to handle noise points, so the

Table 2 Comparison of 3D simulation results with rotation

Datasets	Error	Algorithms			
		ICP	HaICP	MccICP	OURS
Rugby	ε_R	7.80	7.82	0.30	1.86e-04
	$\varepsilon_{\overrightarrow{t}}$	1.78	1.69	0.05	4.09e-05
Food can	ε_R	7.86	7.86	0.60	1.75e-04
	$\varepsilon_{\overrightarrow{t}}$	1.44	1.44	0.12	2.87e-05
Soda can	ε_R	7.79	7.79	0.67	1.19e-04
	$\varepsilon_{\overrightarrow{t}}$	1.58	1.58	0.14	1.62e-05
Soda can 2	ε_R	7.84	7.85	0.72	3.41e-03
	$\varepsilon_{\overrightarrow{t}}$	1.60	1.60	0.16	8.62e-05

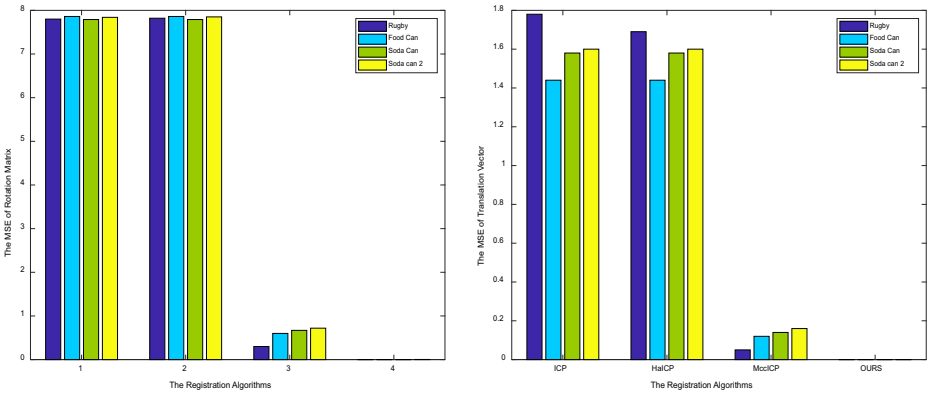

(a) (b)

Fig. 10 The registration results. **a** The MSE of rotation matrix. bb The MSE of translation vector

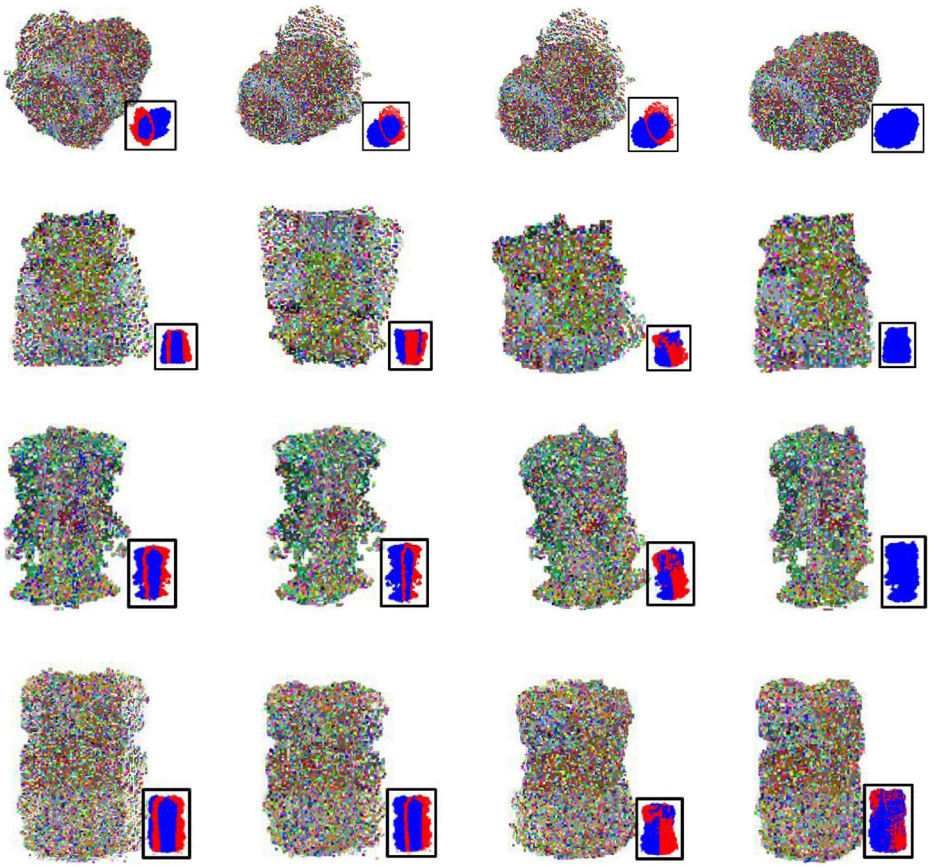

(a) (b) (c) (d)

Fig. 11 The registration results. **a** ICP. **b** HaICP. **c** MccICP. **d** OURS

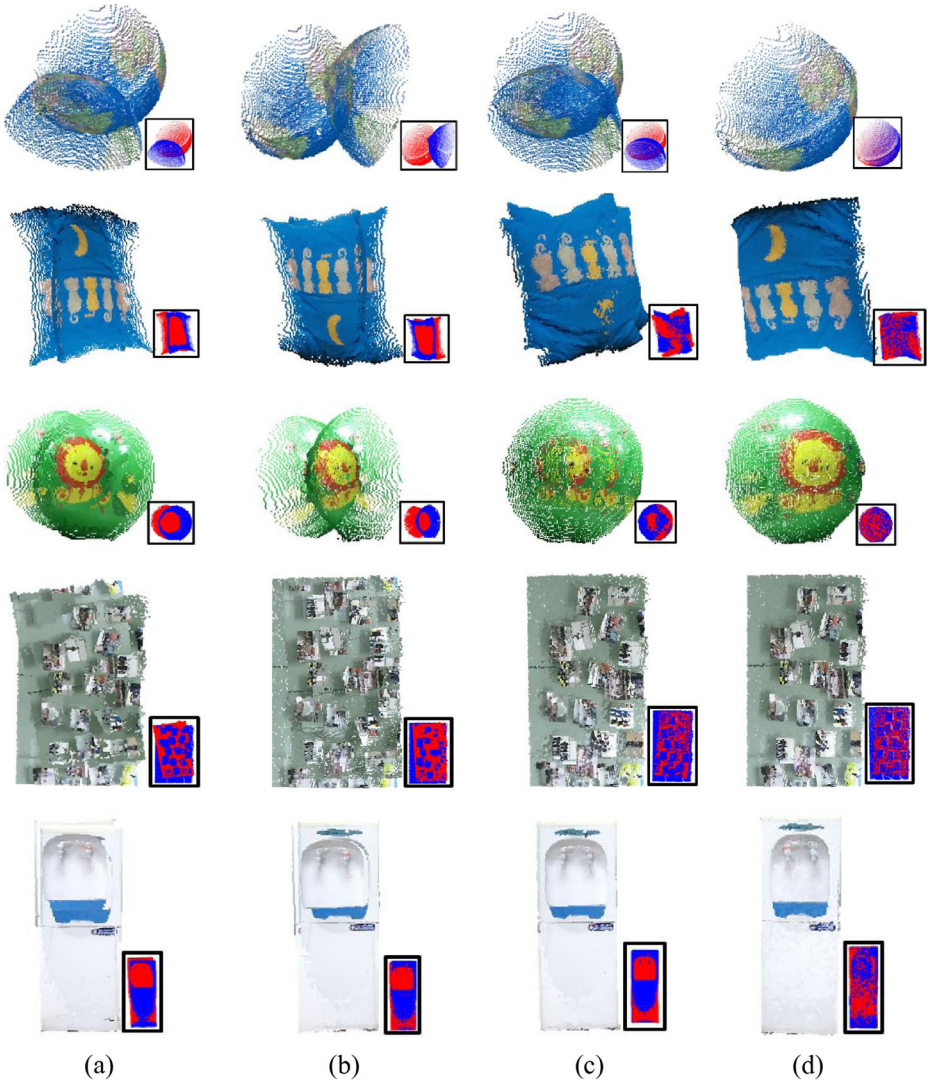

Fig. 12 The registration results with real point sets. **a** ICP. **b** HaICP. **c** MccICP. **d** OURS

HaICP also obtain the incorrect or inprecise registration results. Thirdly, MccICP algorithm can solve the noises and outliers well, but the correspondences between two point sets are incorrect without color guided, which is similar to the ICP algorithm. Therefore, the MccICP algorithm still cannot obtain the correct registration results. Finally, in our algorithm, the correct correspondences between two point sets can be found with coordinate and color information, and the MCC can effectively reduce the impact of noises and outliers on registration results. Therefore, our algorithm obtains the most accuracy and robustness registration results.

In addition, to demonstrate our algorithm have good robustness to noises and outliers, we add random color points into the data and target point sets respectively. The registration results and analysis are shown in Table 2 and Fig. 10.

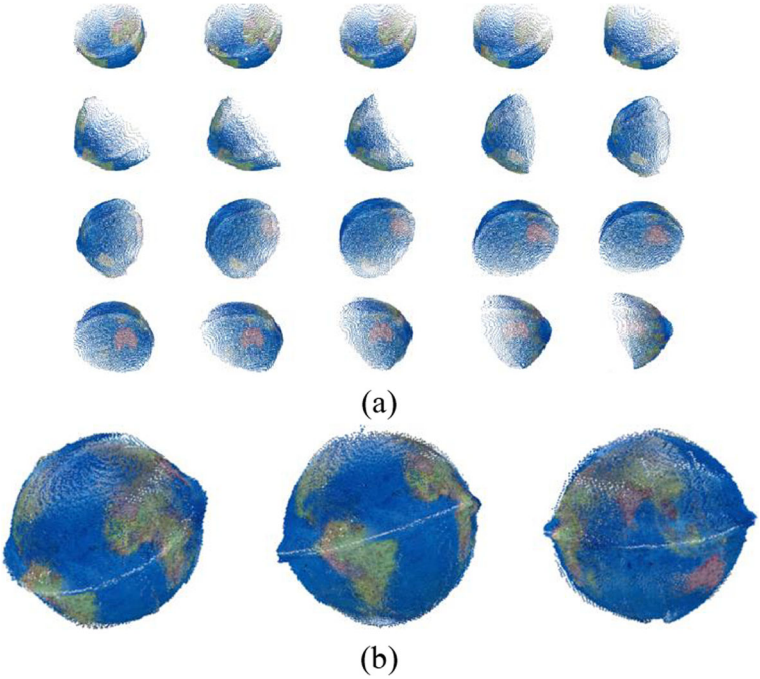

Fig. 13 The objective registration results. **a** The registration results of each two adjacent point set. **b** The reconstruction results

Compared with registration error in Tables 1 and 2, our algorithm still get the most precise registration results than others, because the interference random color noise points and the accuracy of algorithm is reduced. Due to the MSE based measure, the ICP and the HaICP algorithms does not handle noises and outliers well, so they could not obtain good results. The MccICP algorithm has good resistance to noises and outliers,but it still cannot get the accurate and robust results without the color guided because the incorrect correspondences between two points sets are established by the Euclidean distance only. In our algorithm, the color guided ensures the reasonable correspondences can be created in both Euclidean and color space. Moreover, the correntropy reduces the influence of noises and outliers to registration accuracy, so our algorithm can still obtain more accurate experimental results when the point sets contain random noise points. The more intuitive results are shown in Fig. 11.

5.2 Experiments with real data

To verify our algorithm's ability of solving the weak structure point set registration problem. In this section, we test our algorithm with weak structure real data, like surface and hemisphere. We use Microsoft Kinect V2.0 to collect the RGB-D data of objects, and compare our algorithm with the ICP, HaICP and MccICP algorithms. The registration results are show in Fig. 12.

In real data experiment, the ICP algorithm cannot align two hemispherical point sets well because of the incorrect correspondences. The HaICP algorithm could deal with the shape and color information together, but it could not deal with the noises and outliers, which may get the inaccuracy results. Moreover, the MccICP algorithm could not tackle the color information,

the registration failed easily. In our algorithm, the correct correspondences are established with color guided and the noises and outliers are restrained by MCC, so our algorithm obtains the best registration results.

In addition, we reconstruct the objects with our algorithm. Here, we use the dataset of globe and calculate the rigid transformation via registering each two neighboring point sets. Repeat this process until the whole globe is rebuilt as shown in Fig. 13. The structure of each face is weak and similar on the globe, but the color information is abundant and plentiful. Therefore, our algorithm can register two adjacent point sets well and the reconstruction results are good.

6 Conclusion

In this paper, we use the RGB-D information of the smooth surface obtained by multi-source sensors for point set registration. Firstly, traditional registration methods cannot effectively handle weak structure point set. Therefore, we introduce the color information into registration model. Secondly, the maximum correntropy criterion is used to reduce the impact of noises and eliminate the outliers. Thirdly, the ICP-like algorithm is proposed to solve the objective function and the convergence of the algorithm is proved. Finally, the simulation and real data experiments proof that our algorithm can align two smooth surfaces well. Furthermore, we will extend the proposed algorithm to realize the reconstruction of large-scale scenes.

Acknowledgements This work was supported by the National Natural Science Foundation of China under Grant Nos. 61627811 and 61573274, the Fundamental Research Funds for the Central Universities under Grant Nos. xjj2017005 and xjj2017036, Fujian Provincial Key Laboratory of Information Processing and Intelligent Control (Minjiang University) under Grant No. MJUKF-IPIC201802.

References

1. Arun KS, Huang TS, Blostein SD (1987) Least-squares fitting of two 3-d point sets. IEEE Trans Pattern Anal Mach Intell 9(5):698–700
2. M. S. Belshaw and M. A. Greenspan (2008) A high speed iterative closest point tracker on an FPGA platform. In: Proc. IEEE International Conference on Computer Vision Workshops, pp. 1449–1456
3. Benjemaa R, Schmitt F (1997) Fast Global Registration of 3D Sampled Surfaces using a Multi-Z-Buffer Technique. Image Vis Comput 17(2):113
4. Besl PJ, Mckay ND (1992) A method for registration of 3-D shapes. IEEE Trans Pattern Anal Mach Intell 14:239–256
5. Censi A (2008) An ICP variant using a point-to-line metric. In: Proc. IEEE International Conference on Robotics and Automation, pp. 19–25
6. Chetverikov D, Stepanov D, Krsek P (2005) Robust Euclidean alignment of 3D point sets: the trimmed iterative closest point algorithm. Image Vis Comput 23(3):299–309
7. Danelljan M, Meneghetti G, Khan FS, Felsberg M (2016) A Probabilistic Framework for Color-Based Point Set Registration. In: Proc. Computer Vision and Pattern Recognition, pp. 1818–1826
8. Davison AJ, Reid ID, Molton ND, Stasse O (2007) MonoSLAM: real-time single camera SLAM. IEEE Trans Pattern Anal Mach Intell 29(6):1052–1067
9. Du S, Cui W, Wu L, Zhang S, Zhang X, Xu G, Xu M (2017) Precise iterative closest point algorithm with corner point constraint for isotropic scaling registration. Multimedia Systems 9:1–8
10. Du S, Liu J, Bi B, Zhu J, Xue J (2016) New iterative closest point algorithm for isotropic scaling registration of point sets with noise. J Vis Commun Image Represent 38(CAC):207–216
11. Du S, Liu J, Zhang C, Zhu J, Li K (2015) Probability iterative closest point algorithm for m -D point set registration with noise. Neurocomputing 157(CAC):187–198
12. Faugeras OD, Hebert M (1986) The Representation, Recognition, and Positioning of 3-D Shapes from Range Data. Machine Intelligence & Pattern Recognition 3:13–51

13. Fitzgibbon AW (2003) Robust registration of 2D and 3D point sets. Image Vis Comput 21(13):1145–1153
14. Granger S, Pennec X (2002) Multi-scale EM-ICP: A Fast and Robust Approach for Surface Registration. In: Proc. Computer Vision - ECCV 2002, European Conference on Computer Vision, Copenhagen, Denmark, Proceedings, pp. 418–432
15. Greenspan M, Yurick M (2003) Approximate K-D Tree Search for Efficient ICP. In: Proc. International Conference on 3-D Digital Imaging and Modeling, pp. 442–448
16. He Y, Liang B, Yang J, Li S, He J (2017) An Iterative Closest Points Algorithm for Registration of 3D Laser Scanner Point Clouds with Geometric Features. Sensors 17(8):1862
17. Horn BKP (1998) Closed-form solution of absolute orientation using unit quaternions. Journal of the Optical Society of America, Series A 5(7):1127–1135
18. Izadi S, Stamminger M (2013) Real-time 3D reconstruction at scale using voxel hashing. ACM Trans Graph 32(6):169
19. Kaneko S, Kondo T, Miyamoto A (2003) Robust matching of 3D contours using iterative closest point algorithm improved by M-estimation. Pattern Recogn 36(9):2041–2047
20. Kim D, Kim D (2010) A Fast ICP Algorithm for 3-D Human Body Motion Tracking. IEEE Signal Processing Letters 17(4):402–405
21. Korn M, Holzkothen M, Pauli J (2015) Color supported generalized-ICP. In: Proc. International Conference on Computer Vision Theory and Applications, pp. 592–599
22. Lai K, Bo L, Ren X, Fox D (2011) A large-scale hierarchical multi-view RGB-D object dataset. In: Proc. IEEE International Conference on Robotics and Automation, pp. 1817–1824
23. Masuda T, Yokoya N (1995) A robust method for registration and segmentation of multiple range images. CVIU 61(3):106–113
24. Men H, Gebre B, Pochiraju K (2011) Color point cloud registration with 4D ICP algorithm. In: Proc. IEEE International Conference on Robotics and Automation, pp. 1511–1516
25. Myronenko A, Song X (2010) Point Set Registration: Coherent Point Drift. IEEE Transactions on Pattern Analysis & Machine Intelligence 32(12):2262–2275
26. Nchter A, Kai L, Hertzberg J (2007) Cached k-d tree search for ICP algorithms. In: Proc. International Conference on 3-D Digital Imaging and Modeling, pp. 419–426
27. Ridene T, Goulette F and Ois (2009) Registration of fixed-and-mobile- based terrestrial Laser data sets with DSM. In: Proc. IEEE International Symposium on Computational Intelligence in Robotics and Automation, pp. 375–380
28. S. Rusinkiewicz and M. Levoy (2002) Efficient Variants of the ICP Algorithm. In: Proc. International Conference on 3-D Digital Imaging and Modeling, Proceedings, pp. 145–152
29. Schneiderman H, Nashman M (2002) A discriminating feature tracker for vision-based autonomous driving. IEEE Trans Rob Autom 10(6):769–775
30. Silva L, Bellon ORP, Boyer KL (2005) Precision range image registration using a robust surface interpenetration measure and enhanced genetic algorithms. IEEE Transactions on Pattern Analysis & Machine Intelligence 27(5):762–776
31. Sturm J, Engelhard N, Endres F, Burgard W, Cremers D (2012) A benchmark for the evaluation of RGB-D SLAM systems. In: Proc. IEEE/RSJ International Conference on Intelligent Robots and Systems, pp. 573–580
32. Wachowiak MP, Smolikova R, Zheng Y, Zurada JM, Elmaghraby AS (2004) An approach to multimodal biomedical image registration utilizing particle swarm optimization. Evolutionary Computation IEEE Transactions on 8(3):289–301
33. Walker MW, Shao L, Volz RA (1991) Estimating 3-D location parameters using dual number quaternions. Cvgip Image Understanding 54(3):358–367
34. Xu G, Du S, Xue J (2016) Precise 2D point set registration using iterative closest algorithm and correntropy. In: Proc. International Joint Conference on Neural Networks, pp. 4627–4631
35. Yan P, Bowyer KW (2005) A Fast Algorithm for ICP-Based 3D Shape Biometrics. In: Proc. Automatic Identification Advanced Technologies, 2005. Fourth IEEE Workshop on, pp. 213–218

Teng Wan received his Bachelor degree in electrical engineering and automation in 2012 and received his Master degree in Power System and Automation in 2017 from LanZhou University Of Technology. He is currently a Doctoral student in Control Science and Engineering from Xi'an Jiaotong University, China. His research interests include computer vision, pattern recognition.

Shaoyi Du received double Bachelor degrees in computational mathematics and in computer science in 2002 and received his MS degree in applied mathematics in 2005 and PhD degree in pattern recognition and intelligence system at Xi'an Jiaotong University. He was a postdoc research fellow in computer science in Xi'an Jiaotong University from 2009 to 2011, and a visiting scholar at the University of North Carolina at Chapel Hill from 2013 to 2014. He is currently a professor in Institute of Artificial Intelligence and Robotics at Xi'an Jiaotong University. His research interests include image registration, intelligence vehicle, medical image analysis, face image analysis.

Yiting Xu received her Bachelor degree from Northwestern Polytechnical University in 2017. She is currently a master student in the institute of Artificial Intelligence and Robotics in Xi'an Jiaotong University. Her research interests include computer vision, pattern recognition.

Guanglin Xu received his Bachelor degree from Xi'an Jiaotong University in 2016. He is currently a master student in the institute of Artificial Intelligence and Robotics in Xi'an Jiaotong University. His research interests include computer vision, pattern recognition.

Zuoyong Li received the B.S. and M.S. degrees in Computer Science and Technology from Fuzhou University, Fuzhou, China, in 2002 and 2006, respectively. He received the Ph.D. degree from the School of Computer Science and Technology at Nanjing University of Science and Technology, Nanjing (NUST), China, in 2010. He is currently a professor in Department of Computer Science of Minjiang University, Fuzhou, China. He has published over 60 papers in international/national journals. His current research interest is image processing, pattern recognition and machine learning.

Badong Chen received the B.S. and M.S. degrees in control theory and engineering from Chongqing University, in 1997 and 2003, respectively, and the Ph.D. degree in computer science and technology from Tsinghua University in 2008. He was a Postdoctoral Researcher with Tsinghua University from 2008 to 2010, and a Postdoctoral Associate at the University of Florida Computational NeuroEngineering Laboratory (CNEL) during the period October, 2010 to September, 2012. During July to August 2015, he visited the Nanyang Technological University (NTU) as a visiting research scientist. He also served as a senior research fellow with The Hong Kong Polytechnic University from August to November in 2017. Currently he is a professor at the Institute of Artificial Intelligence and Robotics (IAIR), Xi'an Jiaotong University. His research interests are in signal processing, information theory, machine learning, and their applications to cognitive science and neural engineering.

Yue Gao is currently an associate professor in School of Software, Tsinghua University, Beijing, China. He received his B.E. degree in Department of Electronic Information Engineering, Harbin Institute of Technology, his Master Degree and his Ph.D. degree in School of Software and Department of Automation of Tsinghua University, respectively. He has been working in School of Computing, National University of Singapore and School of Medicine, University of North Carolina at Chapel Hill from 2012 to 2016. He is the recipient of the 1000 Youth Talent Plan Grant of China. His research falls in the field of computer vision, medical image analysis, machine learning and its applications.